Chemistry and Physics of Lipids 224 (2019) 104763

Contents lists available at ScienceDirect

Chemistry and Physics of Lipids

journal homepage: www.elsevier.com/locate/chemphyslip

pH responsive delivery of lumefantrine with calcium phosphate nanoparticles loaded lipidic cubosomes for the site specific treatment of lung cancer

Vaidevi Sethuraman, Kumar Janakiraman, Venkateshwaran Krishnaswami, Subramanian Natesan, Ruckmani Kandasamy*

Centre for Excellence in Nanobio Translational REsearch (CENTRE), Department of Pharmaceutical Technology, University College of Engineering, Anna University, BIT Campus, Tiruchirappalli, Tamil Nadu, India

ARTICLE INFO

Keywords:
Lumefantrine
Cubosomes
Lung cancer
Cytotoxicity

ABSTRACT

The present work aim to develop pH responsive nanosystem comprising lumefantrine with calcium phosphate nanoparticles loaded lipidic cubosomes for the effective treatment of lung cancer. FTIR results showed that, compatibility nature of selected excipients for the synthesis of LF-CaP-Cs. The XRD results showed developed LF-CaP-Cs were non crystalline in nature. The selected developed LF-CaP-Cs were in cubic phase with average particle size of 259.4 ± 19 nm with a charge of -2.28 ± 0.7 mV. The encapsulation efficiency for LF within LF-CaP-Cs was about 78.76 ± 0.5%. RP-HPLC analysis showed that LF release rate gets significantly enhanced with higher peak area at pH 4.0 compared to pH 5.0/pH 7.4. The *in-vitro* release of LF-CaP-Cs showed that LF release gets significantly increased at pH 4.0 (84.04 ± 0.4%) compared to pH 7.4 (48.32 ± 1.6%) at 12 h. Further, CAM assay showed the superior anti-angiogenesis potential of developed LF-CaP-Cs compared to LF-Cs/blank Cs. The cytotoxicity effect of LF-CaP-Cs (28 ± 1.8 µg/mL) was significantly higher than that of free LF (40 ± 0.9 µg/mL). The results of cellular uptake study proved the localization of LF at cellular level and AO/EB staining results revealed that the A549 cell undergoes apoptosis in A549 cells.

1. Introduction

Lung cancer is characterized by uncontrolled growth of cells in tissue/cells in lungs. Thereby, the cancer cells spreads to nearby tissues or cells through metastasis. Lung cancer is the leading cause of cancer-associated mortality globally, with a low survival rate (both in men's and women's). The prevalence of lung cancer globally results with 1.38 million cancer death per year, which estimates more deaths than any other type of cancer (Ridge et al., 2013). The major types of lung cancer were small cell lung carcinoma (SCLC) and non-small cell lung carcinoma (NSCLC). NSCLC accounts for 87% of lung cancer cases globally with its most common subtypes such as squamous cell carcinoma, large cell carcinoma and adenocarcinoma. The symptoms associated with NSCLC includes cough, chest pain, shortness of breath, coughing up blood, wheezing, hoarseness, recurring infections such as bronchitis and pneumonia, weight loss, loss of appetite and unusual fatigue. The major molecular pathways involved in lung cancer are kirsten rat sarcoma viral oncogene and epidermal growth factor receptor pathways both in smoker and non-smoker patients (Sethi et al., 2012). But, smoking seems to be major risk factor and leading cause (80%) for lung cancer. The radon remains the second most independent risk factor for lung cancer which predominantly affects the persons working in mine industries (Turner et al., 2011; Nielsen et al., 2014). Silicate type of asbestos present in soil and rocks also acts as an environmental carcinogenic agent for the development of lung cancer (Mani et al., 2012). The other possible risk factors include HIV infection, tuberculosis, emphysema, pulmonary diseases and environmental factors such as beryllium, nickel, copper, cadmium (Denholm et al., 2014; Powell et al., 2013; Yu et al., 2011; Amreddy et al., 2017). The conventional treatment option for lung cancer includes surgery, radiotherapy, stem cell transplantation, immunotherapy, gene therapy and chemotherapy. The limitations of these treatment options were poor therapeutic efficiency, non-specific interactions, toxicity to normal tissues and multi-drug resistance which creates major obstacle for lung cancer treatment (Noronha et al., 2016).

In recent years, researchers are developing various nano particulate

* Corresponding author at: Centre for Excellence in Nanobio Translational REsearch (CENTRE), Department of Pharmaceutical Technology, University College of Engineering, Anna University, BIT Campus, Tiruchirappalli, 620 024, Tamil Nadu, India.
E-mail address: ruckmani@aubit.edu.in (R. Kandasamy).

https://doi.org/10.1016/j.chemphyslip.2019.03.016
Received 28 November 2018; Received in revised form 11 March 2019; Accepted 30 March 2019
Available online 02 April 2019
0009-3084/

systems which acts as carriers for the effective treatment of lung cancer and this may overcome the limitations associated with conventional treatment strategies (Yaghmur and Glatter, 2009). Cubosomes (Cs) are cubic liquid phase crystalline nanoparticle with bi-continuous phase consisting of lipid and water (Pan et al., 2013). Cs holds better drug loading properties due to its higher surface area, stable characteristics, viscous nature, bio-adhesivity and biocompatibility (Peng et al., 2010). Cs showed significant advantages towards loading of hydrophobic/hydrophilic/amphiphilic type of drugs (Lee et al., 2009; Nasr et al., 2015). Different categories precursors and emulsifiers were widely used for the preparation of Cs. Recently, cubosomal based nanoparticle were reported to load anti-cancer drugs such as 5-fluorouracil, doxorubicin, etoposide and etodolac, capsaicin, resveratrol (Abdel-Bar and EL Basset, 2017; Tian et al., 2017). Folate modified Cs loaded with etoposide with sustained release pattern and it was reported for the treatment of breast cancer (Bilewicz et al., 2017). Cs loaded with doxorubicin was reported as pH sensitive carrier for anti-cancer treatment (Zhen et al., 2012). Similarly, it was reported that, Cs used for siRNA delivery and gene silencing (Kim and Leal, 2015). Steric stabilized bicontinuous cubic PEGylated Cs were reported to deliver siRNA with higher transfection efficiency (Aweeka and German, 2008)

Lumefantrine (LF) otherwise known as benflumetol, is a yellow coloured, lipophilic fluorine (benzindene) derivative, chemically termed as (a-(dibutylaminomethyl)-2,7-dichloro-9-(p-chlorobenzylidene)-5-fluorenemethanol). LF possesses aryl-amino alcohol with properties similar to other antimalarials (quinine, halofantrine, mefloquine) (Kokwaro et al., 2007). As an antimalarial drug, LF prevents detoxification of heam, thereby the toxic heam and free radicals induce parasite death (Ezzet, 2000). LF is poorly soluble in water, oils, but soluble in chloroform, unsaturated fatty acids and acidified organic solvents. The absorption of LF occurs at 2 h after oral administration which reaches peak at 3–4 h (White, 1999). The peak plasma LF level was found at 6–8 h after administration whereby, plasma LF levels reported to vary considerably between individuals (Travassos and Laufer, 2009). LF holds half-life of 3–6 days. LF mostly bond to plasma proteins especially with high density lipoproteins (HDL). The drug delivery problems associated with LF were poor bioavailability and low solubility in aqueous media or physiological buffers. Recently, LF and its derivatives have been reported for cancer treatment (autophagy inhibitor in BAF3 cell line) (McKenzie, 2011).

Calcium phosphate nanoparticles (CaP) are recently holding much interest in cancer drug delivery due to its biocompatibility, biodegradability and higher drug loading efficiency (Khan et al., 2016). It has been reported that, growth of the CaP gets controlled during synthetic approaches and by w/o emulsion based synthetic approaches (Roy et al., 2003). CaP has the capacity to transport in to different biomolecules such as proteins, nucleic acids, gene or antigens across the cell membrane effectively (Hadjicharalambous et al., 2015; Lee et al., 2014; Sahdev et al., 2013; Rotan et al., 2017). CaP was taken up effectively by cells via endocytosis and more specifically by micropinocytosis, which paves way to deliver drugs/molecules across endosomes and subsequently into lysosomes (Sokolova et al., 2013). CaP are easily taken up by cells within short duration, dissolved in the lysosome and finally excreted in ionic form (Neumann et al., 2009). CaP has been also used for *in-vitro* cell transfection due to its high biocompatibility. CaP elicits stimuli responsive behavior and this strategy has been used for drug delivery applications. As a pH responsive behavior CaP gets dispersed at acidic pH (both endosomal/lysosomal pH) thereby the osmotic pressure inside the cellular compartments gets increased thereby leads to endosomal escape (Rim et al., 2011). Synthetic approaches for CaP synthesis is attractive due to its simple preparation methods and usage of less expensive precursors (Zhang et al., 2009; Schwiertz et al., 2009).

Biological macromolecules play a major role in drug delivery and cancer therapeutics due to its distinct features such as biocompatible and non-immunogenic nature (Sezaki and Hashida, 2011). Macromolecule based drug delivery system enable to deliver therapeutic molecules/proteins through invasive (intravenous, subcutaneous and intramuscular injections) and non-invasive (transdermal, pulmonary, oral, buccal and ocular) routes (Jitendra et al., 2011). Nanotechnology supports efficacy of macromolecules and thereby it reduces the dose/frequency of administration of therapeutic drugs. Poloxamer 188 is a FDA approved, non-ionic surfactant based macromolecule (molecular weight - 8400 Da) characterized by its properties such as biodegradable, thermo sensitive, non-immunogenic, biocompatible nature consisting of polyethylene-propylene glycol widely used for nano based drug delivery systems which acts as solubilizer, emulsifier and stabilizer (Santander-Ortega et al., 2007; Zarrintaj et al., 2018). Poloxamer 188 is soluble in aqueous, polar and nonpolar organic solvents. Due to its thermo reversible property, poloxamer forms a gel like structure. Poloxamer 188 has been reported to overcome multidrug resistance in breast cancer cells by inhibiting p-glycoprotein efflux. Nanoparticles coated with poloxamer enhances the plasma residence time of drugs in biological systems (Semete et al., 2010, 2012). Poloxamer 188 coated nanoparticle improve the drug delivery to lymph nodes which improves the lymphatic uptake compared to uncoated nanoparticle (Gaymalov et al., 2009). Surface coating with poloxamer 188 modifies the hydrophobic drug carriers by reducing the surface charge thereby prevents opsonization and improve the blood residence time (Bodratti and Alexandridis, 2018). Poloxamer 188 hinders the initial burst release of drug molecule thereby provides controlled drug release pattern (Sharma et al., 2016). The pore forming capacity of poloxamer 188 enhances the loaded drug release characteristics. Poloxamer 188/poly (ε-caprolactone) nanoparticle loaded with paclitaxel has been reported for the treatment of breast cancer where poloxamer 188 act to enhance the paclitaxel release by acting as pore forming agent (Shubhra et al., 2014). Poloxamer 188 based curcumin loaded micelles prepared using pol by thin film hydration technique showed better solubility for curcumin and exhibited better cytotoxic effect in MCF-7 cells (Tian et al., 2010). Heparin - poloxamer 188 conjugates used for protein delivery application (Noronha et al., 2016). In the present work, CaP based cubosomes provide site specific delivery of LF to lung cancerous cells (slightly acidic environment). We hypothesized that the LF with calcium phosphate nanoparticle loaded cubosomes (LF-CaP-Cs) may enhance the site specific delivery of LF for the treatment of lung cancer due to the pH responsive characteristics of CaP. As an antimalarial drug (LF) this is first report to show the pH responsive characteristics of LF-CaP-Cs.

2. Materials and methods

2.1. Materials

Lumefantrine was obtained as a gift sample from Madras Pharma, Chennai. Chloroform, methanol, acetonitrile, cetyl palmitate, poly vinyl alcohol, calcium chloride, sodium dodecyl sulphate, potassium dihydrogen phosphate, sodium citrate, poloxamer 188, tween 80, sodium chloride, potassium chloride, magnesium sulphate were purchased from TCI Chemicals, Tokyo. All buffers and solutions were prepared using Milli Q water.

2.2. Synthesis of calcium phosphate nanoparticles (CaP)

Aqueous calcium chloride solution 0.05 M was treated with sodium dodecyl sulphate (1%) and poloxamer 188 dissolved (1.0%) and stirred for 300 rpm for 24 h to form microemulsion (Solution A). Potassium dihydrogen phosphate (0.025 M), sodium citrate (0.025 M), SDS (1%), poloxamer 188 (1%) was stirred at 37 °C for 24 h (Solution B). The solution B was injected in to solution a drop wise, stirred for 300 rpm (24 h). The resultant nanoparticles were centrifuged at 15,000 rpm for 15 min. The Pelleted nanoparticles were washed thrice with ethanol. The prepared CaP was freeze dried and stored for further analysis.

2.3. Characterization of calcium phosphate nanoparticles (CaP)

Scanning electron microscopy (SEM) images and the energy dispersive X-ray (EDX) spectrum of CaP were recorded using XL30 ESEM-FEG field-emission scanning electron microscope (FEI Co).

2.4. Development of LF-CaP-Cs

LF-CaP-Cs was prepared using cetyl palmitate, poloxamer 188, poly vinyl alcohol (0.125 − 0.25%), CaP and lumefantrine (LF) by emulsification along with homogenization technique. Briefly, 5–10 mg of cetyl palmitate was melted at 60 °C and 10 mg of poloxamer 188 was added to above melted lipid phase. Further, CaP and 2 mg of LF was added along with the above lipid phase. PVA solution (0.125%) was used as aqueous phase for the formulation development. The above aqueous phase was treated to the lipid phase by maintaining the temperature (60 °C) at 20,000 rpm for 20 min. using high pressure homogenizer (T25 homogenizer, IKA). Formulation parameters such as cetyl palmitate ratio, poloxamer 188 concentration and poly vinyl alcohol were varied and best formulations were selected based on higher drug loading and lower size. Similarly, LF-Cs and blank Cs were also prepared.

2.5. In-vitro characterization of LF-CaP-Cs

Particle size and charge of LF-CaP-Cs were performed by Malvern zeta sizer (Malvern NANO ZS series). The morphology of LF-CaP-Cs was checked using high resolution transmission electron microscopy (hr-TEM- Jeol/JEM 2100). Crystallinity behavior of LF-CaP-Cs was checked using X-ray diffractometer (Panalytical/X'Pert Pro). The compatibility of cetyl palmitate, poloxamer 188, LF, poly vinyl alcohol and CaP present the formulation was recorded using FTIR spectrophotometer (JASCO/FTIR-6300, Japan). For FTIR samples were prepared by KBr pellet method using hydraulic pellet press and scanned over a range of 4000 cm^{-1} to 400 cm^{-1}

2.6. Stability studies for LF-CaP-Cs

In-vitro stability studies were performed for LF-CaP-Cs by storing at different temperature such as, room conditions (37 °C) and refrigerated conditions (5–20 °C) over the period of time 0 h, 24 h and 48 h. Samples were analyzed for its particle size and zeta potential values, after its respective conditions.

2.7. RP-HPLC method for LF estimation

RP-HPLC analysis for the estimation of LF was performed using Shimadzu SPD M20A Ultra Performance Liquid Chromatography equipped with degassing Unit (DGU-20A5R), LC-30AD pump, SIL-30 AC auto sampler, CTO-20 AC prominence column oven and SPD-M20A prominence diode array detector (Spinco Biotech, Chennai, India). The chromatographic separation was achieved using the mobile phase combination of methanol with 0.1% trifluoro acetic acid (TFA) and milli Q water with 0.1% TFA (50:50% v/v) at a flow rate of 0.2 mL/min using Shimpack GIST C8 Column (150 mm × 2.1 mm, 2 µm). The UV detection was performed at 250 nm using photodiode array detector. This method was utilized to check the internal stimuli (pH responsive) behaviour of LF-CaP-Cs.

2.7.1. Preparation of LF standard solution

Standard stock solutions of LF (1 mg/mL) was prepared by dissolving 10 mg of LF in 1 mL of chloroform and sonicated for 5 min and made up to the mark (10 mL) using acetonitrile. Further, dilutions were made (1–5 µg/mL) using pH 7.4 buffer. The resultant solution was filtered (0.22 µm) and utilized for HPLC analysis and linearity was checked.

2.7.2. Internal stimuli responsive behavior of LF-CaP-Cs

Internal stimuli response behavior of LF-CaP-Cs was checked at three different pH (pH 4.0, pH 5.0 and pH 7.4) based phosphate buffers. In order to simulate extra cellular and endolyosomal condition, three different pH buffers with LF-CaP-Cs were employed and checked in HPLC using developed method. Herein, 100 mL of respective buffer was treated with 100 µL of LF-CaP-Cs, maintained at 37 °C and stirred at 600 rpm. At different time intervals (1 h, 2 h and 3 h) samples were withdrawn and replaced with respective buffers and analyzed using HPLC. Samples were filtered (0.22 µm) and injected in to the HPLC.

2.8. Encapsulation efficiency of LF in LF-CaP-Cs

Encapsulation of LF with the LF-CaP-Cs was estimated using UV visible spectrophotometer. Briefly, 100 µL of LF-CaP-Cs was treated with methanol (100 µL), further treated with 0.5% of formic acid in acetonitrile:water (50:50% v/v). Further, dilutions were made using 0.1% tween 80 in phosphate buffer. The mixture was analyzed using UV–vis spectrophotometer (Shimadzu/UV-2000, Japan) at 224 nm.

2.9. In-vitro release behavior of LF-CaP-Cs

The *in-vitro* release study for LF-CaP-Cs was performed using centrifugal method. Herein, 100 µL of LF-CaP-Cs/LF were treated with 0.01% of tween 80 containing 10 mL of phosphate buffer pH 7.4 and 4.0 individually. The samples were kept in shaking incubator at 37 °C maintained at 120 rpm. Samples (2 mL) were collected at different time intervals (0.5 h, 1 h, 1.5 h, 2 h, 3 h, 4 h, 5 h, 6 h, 7 h, 8 h and 12 h) and replaced with same volume (2 mL) of respective phosphate buffer (pH 7.4/pH 4.0) in respective sample. The collected samples were analyzed in UV–vis spectrophotometer at 224 nm. The LF release of LF-CaP-Cs was compared with that of free LF release in pH 7.4 and 4.0 buffer separately.

2.10. Hemolytic potential of LF-CaP-Cs

Blood was collected from wistar albino rat in heparinized tubes and hemolytic potential of the developed LF-CaP- Cs was analyzed using automated cell counter (Vetrinary Hematology Analyzer PE-6800 VET). Briefly, 20 µL of heparinized blood was treated with 1.5 mL of pre-diluent and slightly mixed to form uniform mixture. 20 µL of LF-CaP-Cs at varying concentrations (1000 ng/mL, 100 ng/mL, 10 ng/mL and 1 ng/mL) were treated individually with diluted blood samples and analyzed for its RBC and WBC counts using phosphate buffer saline, triton X-100 as control and positive control respectively. Hemolytic potential was calculated by using following formula

$$Hemolysis\ (\%) = \frac{RBC\ counts\ of\ control - RBC\ counts\ of\ sample}{RBC\ Control\ of\ control} \times 100$$

2.11. Anti-angiogenesis assay (CAM assay)

Chick chorioallantoic membrane (CAM) assay was a well-established method reported to assess the tumor growth and metastasis, toxicity analysis and angiogenesis potential of drug/nanoformulation (Ribatti, 2016). Herein, anti-angiogenesis assay was performed using 8 day old pathogen free embroyanated chick eggs. Fertilized eggs were incubated at 37 °C and maintained with 60% relative humidity. The egg shell was partially removed for about 1 cm at the top during the 8^{th} day. The inner membrane was carefully removed and moistened with 0.9% NaCl. The exposed CAM was treated with 10 µL of each LF-CaP-Cs (10 ng/disc), blank Cs, LF-Cs and saline. After 48 h of treatment, respective discs were removed and CAM vessel morphology was photographed for morphological changes.

Further, FITC labeled LF-CaP-Cs (10 ng/mL) treated CAM vessels were isolated and placed in microscopic slide after 2 h incubation

washed with PBS thrice and observed under microscope (Motic BA 310) using untreated CAM vessels as control.

2.12. Erythrocyte aggregation assay

Erythrocyte aggregation assay was performed to check the toxicity of LF-CaP-Cs upon isolated erythrocyte. About, 1 mL of wistar albino rat blood was collected in heparinized tubes and centrifuged at 6000 rpm for 15 min. to separate erythrocytes. Erythrocyte were washed thrice with PBS (pH 7.4) and further redispersed in PBS. To check the toxic effect of LF-CaP-Cs visually, 100 µL of erythrocytes were incubated with 400 µL of LF-CaP-Cs dispersed in PBS, incubated for 1 h at 37 °C and erythrocytes were imaged at 40x magnification under microscopy (Motic BA 310) using untreated erythrocytes as control.

2.13. Cytotoxicity assay

Cytotoxic effect of LF-CaP-Cs, LF, LF-Cs, CaP-Cs and blank Cs was performed in human lung adenocarcinoma cell line (A549) by MTT assay. Briefly, 5×10^5 cells/well were incubated in dublecco modified eagle's medium (DMEM) medium containing serum (10%), and antibiotics penicillin (1%) in 96 well plates maintained at 37 °C for 24 h supplemented with 5% CO_2. The incubated cells were treated with different concentrations varying (10–100 µg/mL) of LF-CaP-Cs, LF, LF-Cs, and blank Cs were kept for each 24 h and 48 h incubation. Further, the media was removed and 20 µL of MTT (5 mg/mL) was added and incubated for 4 h. The media was removed by DMSO (100 µL) to solubilize formazan crystals. The absorbance of the resultant samples was measured at 570 nm using multimode microplate reader (Perkin Elmer/Enspire) using untreated cells used as control and cytotoxicity (%) was calculated as follows

$$Cytotoxicity\ (\%) = \frac{Absorbance\ of\ test\ sample - Absorbance\ of\ control}{Absorbance\ of\ control} \times 100$$

2.14. In-vitro cellular uptake of LF-CaP-Cs

A549 cells were seeded in 6 well plates at a density of 5×10^5 cells/well in DMEM medium and allowed to adhere for 24 h. After 24 h, the cells were incubated with FITC labelled LF-CaP-Cs for 4 h, 6 h and 12 h and fluorescent image were captured at the excitation (495 nm) and emission (515 nm) wavelength of FITC (Nikon Eclipse Microscope, Japan). To quantify the cellular uptake, the media in the wells were removed and washed with PBS twice. The cells were lysed using triton X-100 and the cellular uptake of FITC labelled LF-CaP-Cs in A549 cells were measured by measuring the fluorescent intensity in cell lysate.

2.15. Acridine orange (AO) and ethidium bromide (EB) staining

Acridine orange (AO) and ethidium bromide (EB) staining was performed and morphology of the cells with respect to apoptosis was evaluated by using this staining technique (Spector et al., 1998). The cell suspension of each sample ($1C_{50}$ concentrations of LF-CaP-Cs, LF, LF-Cs) containing 5×10^5 cells, was treated with 25 µL of AO and EB solution (3.8 µM of AO and 2.5 µM of EB in PBS) and examined under fluorescent microscope (Carl Zeiss, Germany) using an UV filter (450–490 nm). After incubation cells were harvested and washed with cold PBS. The cells were scored as viable, apoptotic/necrotic as judged by the staining; nuclear morphology and membrane integrity. The percentages of apoptotic/necrotic cells were calculated and morphological changes were imaged.

2.16. Data analysis

The student *t*-test was applied for evaluating possible statistical differences among the groups. A P-value less than 0.05 were considered to be statistically significant. Few graphs were obtained by using Origin 7.0 software (OriginLab Corporation, USA). Zeta potential graph and particle size distribution were obtained directed from the Zetasizer software (Malvern, USA).

3. Results and discussion

3.1. Solubility of LF in lipids

The solubility of LF in different lipids such as tripalmitin, tristearin, stearic acid, cetyl palmitate, follows the order of tripalmitin (0.054 mg/mL) > tristearin (0.657 mg/mL) > stearic acid (0.822 mg/mL) > cetyl palmitate (0.952 mg/mL). Among, which cetyl palmitate showed higher solubility for LF compared to other lipids hence cetyl palmitate has been selected for further studies. Maximum solubility of drug in lipid phase may elicit higher drug loading with maximum release of drug at target site of action (Rosenblatt and Bunjes, 2017)

3.2. Fourier infrared spectroscopy analysis

Fourier infrared spectroscopy used to study compatibility/interaction/structural and functional groups alterations of excipients and LF used in formulation. The appearance and disappearance or shift in peaks indicates there is interaction between lumefantrine and excipients used in formulation. Cetyl palmitate showed characteristic peaks at 2920 cm^{-1} and 1732 cm^{-1} corresponds to OH acid and C═O ester group respectively. Further, cetyl palmitate shows 1183 cm^{-1} and 725 cm^{-1} corresponds to C—O and C—H methyl group. In case of poloxamer 188 shows peak at 2886 cm^{-1} and 1351 cm^{-1} corresponds to OH functional group and N—H stretching vibrations. Further, peaks at 952 cm^{-1} show C—H bending vibrations. In case of PVA, it shows peak at 1989 cm^{-1}, 2885 cm^{-1}, which corresponds C—H Group, OH acid. LF shows characteristic peak at 3398 cm^{-1} and 2951 cm^{-1} corresponds to OH stretching and C—H stretching vibarations. 1442.1 cm^{-1} corresponds to C—H bending vibration and a peak ranging from 830 to 890 cm-1 corresponds to C—Cl group of lumefantrine. The absence of LF characteristic peaks in LF-CaP-Cs shows that LF is compatible and its gets encapsulated within the Cs (Fig. 1a).

3.3. Development of LF-CaP-Cs

LF-CaP-Cs was prepared through emulsification coupled with high pressure hot homogenization technique. CaP utilized for the formulation has been synthesized using nano precipitation technique. The EDAX result showed that amount of calcium present within calcium phosphate nanoparticle was found to be 8.41% w/w of calcium whereas, the amount of phosphate present within the calcium phosphate nanoparticle was found to be 3.39% w/w (Fig. 1d). The amount of CaP present with in the LF-CaP-Cs was found to be 0.17 g/mL. By altering the cetyl palmitate concentration (5 and 10 mg), poloxamer 188 concentration (10 mg and 15 mg) and PVA concentration (0.125% and 0.25%) different trials were prepared (LF-CaP-Cs -1 to LF-CaP-Cs-6). Herein, PVA used in the LF-CaP-Cs may reduce the size of particles with low poly dispersity index and uniform distribution. Thereby, PVA acts as stearic barrier/stabilizer and prevents aggregation of Cs. Poloxamer 188 acts as a non-ionic surfactant/stabilizing agent. It has been reported that, increasing the concentration of poloxamer 188 in the LF-CaP-Cs decreases the droplets size by increasing the interfacial stability of LF-CaP-Cs (Bodratti and Alexandridis, 2018). Previously, 5-fluorouracil loaded Cs were reported using glycerol mono oleate for the treatment of hepta cellular carcinoma (Abdel-Bar and EL Basset, 2017). Folate-modified Cs containing etoposide prepared by high pressure

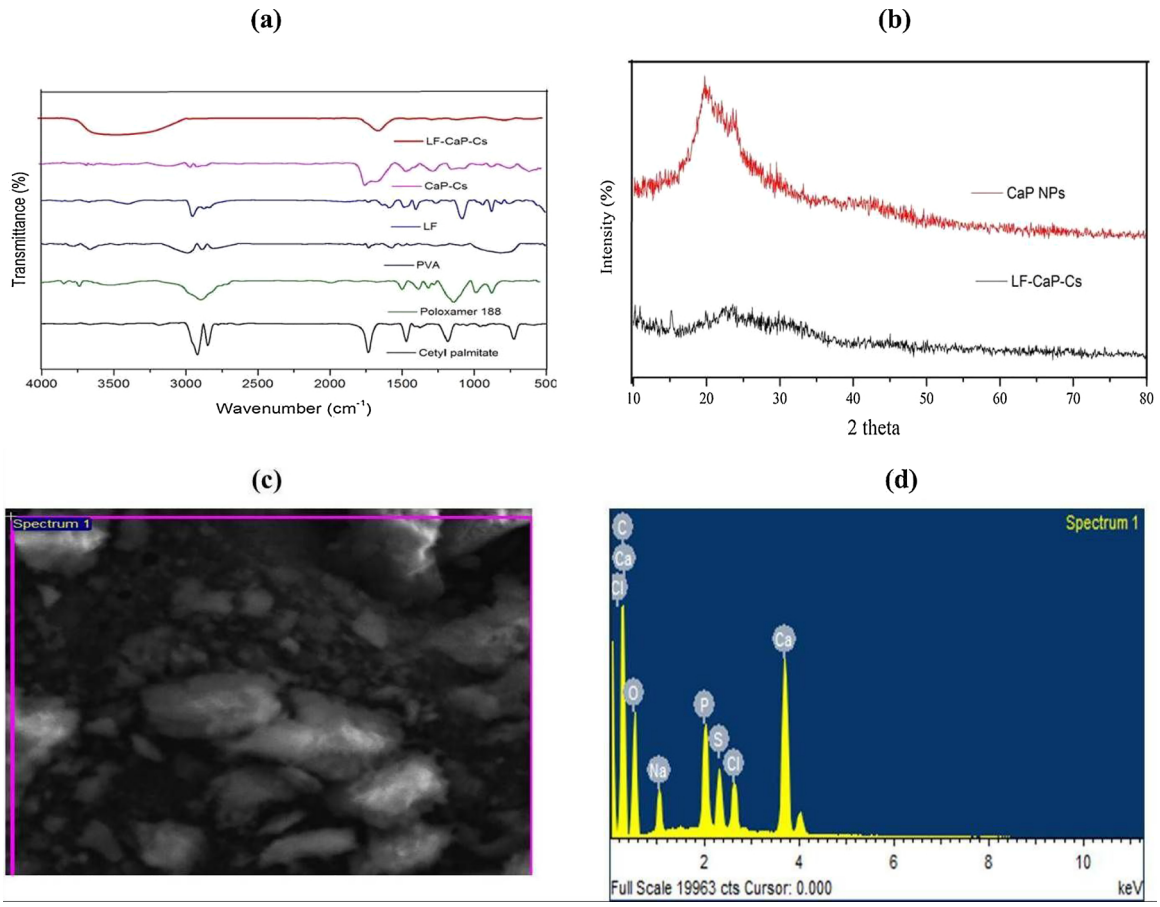

Fig. 1. (a) FTIR spectra of LF-CaP-Cs, CaP-Cs, LF, PVA and cetyl palmitate showed the encapsulating of LF within the LF-CaP-Cs (b) X-ray diffractometric images of CaP and LF-CaP-Cs shows crystalline nature of CaP (c) Scanning electron microscopic image of CaP showing the particles are in dispersed form (d) Energy dispersive x-ray spectroscopy for CaP showed 8.41% w/w of calcium and 3.39% w/w of phosphate content.

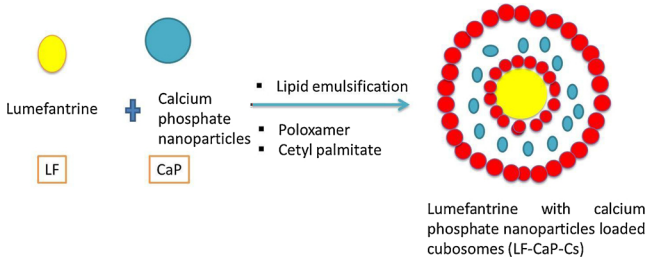

Fig. 2. Schematic illustration of LF-CaP-Cs synthesis by lipid emulsification with high pressure homogenization technique.

homogenization technique was reported for the treatment of breast cancer (Tian et al., 2017). siRNA loaded calcium phosphate loaded poly (lactic-co-glycolic acid) nanoparticles coated with polyethylenimine used to knock down gene expression by RNA interference were also reported for the treatment of pulmonary inflammation (Frede et al., 2017). The schematic representation of LF-CaP-Cs was shown in Fig. 2.

3.4. Particle size and zeta potential analysis

The particle size analysis for LF-CaP-Cs-1 to LF-CaP-Cs-6 showed that particle size varies from 259.4 ± 29–1136 nm ± 15 (Table. 1). Higher percentage of PVA (0.25%) is required to produce Cs with lower particle size compared to lower concentration (0.125%). Further, higher poloxamer 188 concentration (15 mg) is required to produce Cs with lower particle size compared to lower concentration (10 mg). The increase in particle size in few instances may be due to the reduction of interfacial stability that may resulted from insufficient amount of poloxamer 188 for the Cs formation which may leads to cubosomal aggregation (Honary and Zahir, 2013). The poly dispersity index for (LF-CaP-Cs-1 to LF-CaP-Cs- 6) varied from 0.32 to 0.45 ± 0.06 which indicates the monomodal distribution of Cs. Zeta potential of the Cs (LF-CaP-Cs-1 to LF-CaP-Cs-6) was studied to determine the surface charge of the Cs which may determine the long term stability of the colloidal dispersions (Jiang et al., 2009). Herein, the zeta potential of the LF-CaP-Cs- 1 to LF-CaP-Cs-6 varies from -3.58 to -1.41 mV. The pH of prepared LF-CaP-Cs was in the range of 8.23 ± 0.14.

3.5. hr-TEM analysis of LF-CaP-Cs

The hr-TEM image reveals that the developed LF-CaP-Cs-2 were in irregular poly angular shape with cubic morphology without aggregation (Fig. 3 iv)

3.6. Encapsulation efficiency of LF-CaP-Cs

Encapsulation efficiency was calculated for all LF-CaP-Cs-2 formulations and summarized in Table 1. Overall results suggested that, LF-CaP-Cs-2 showed comparatively higher (78.76 ± 0.5%) encapsulation efficiency with lower particle size (259.4 ± 19 nm) and zeta potential (-2.28 ± 0.7 mV). Hence, among the different trials, LF-CaP-Cs-2 has been selected for the further studies with the optimized concentrations of cetyl palmitate (10 mg), poloxamer 188 (15 mg) and 0.125% of PVA in aqueous solution.

Table 1
Particle size, zeta potential, encapsulation efficiency and pH of different formulations (LF-CaP-Cs-1 to LF-CaP-Cs-6).

Formulation code	Poloxamer 188 (mg)	Cetyl palmitate (mg)	PVA ratio (%)	Particle size (nm) ± SD	Zeta potential (mV) ± SD	Encapsulation (%) ± SD	pH ± SD
LF-CaP-Cs-1	10	5	0.125	857.2 ± 23	−3.58 ± 0.4	64.48 ± 1.8	7.98 ± 0.23
LF-CaP-Cs-2	15	10	0.25	259.4 ± 19	−2.28 ± 0.7	78.76 ± 0.5	8.23 ± 0.14
LF-CaP-Cs-3	10	10	0.125	883.9 ± 21	−2.13 ± 0.3	53.07 ± 1.4	8.02 ± 0.12
LF-CaP-Cs-4	15	5	0.125	894 ± 26	−1.41 ± 0.3	63.39 ± 1.25	8.13 ± 0.24
LF-CaP-Cs-5	10	10	0.25	1136 ± 24	−1.91 ± 0.1	88.09 ± 1.3	8.45 ± 0.11
LF-CaP-Cs-6	15	5	0.25	824 ± 21	−3.25 ± 0.3	69.54 ± 0.8	8.56 ± 0.08

3.7. X-ray diffraction studies

The XRD results of CaP showed sharp intense peak at the 2θ of 15.18 and 22.86 with the peak intensity of 100% and 71.36% respectively. Further, LF-CaP-Cs doesn't show any sharp intense peaks indicate non-crystalline nature of LF-CaP-Cs (Fig. 1b).

3.8. In-vitro stability profile for LF-CaP-Cs

Stability studies proved that there is no major difference in particle size/zeta potential values of LF-CaP-Cs over the period of time (0 h, 24 h and 48 h). Generally, it has been reported that Cs are stable at room temperature (He et al., 2017a,b). In room temperature and refrigerated conditions, there were not many variations in particle size values up to 24 h (308.33 ± 8 nm) and 48 h (291.4 ± 12 nm) whereas, there was slight increase in particle size was observed when stored in refrigerated conditions (48 h) (473.7 ± 17 nm). There is a decrease in zeta potential for LF-CaP-Cs at 24 h and 48 h (Fig. 4). The stabilization effect may be afforded due to the presence of poloxamer 188 in the formulation; here, poloxamer 188 acts as stabilizing agent.

3.9. Internal stimuli responsive behavior of LF-CaP-Cs

To check the internal (pH) stimuli responsive behavior of LF-CaP-Cs the developed RP-HPLC has been used maintaining the chromatographic conditions as mentioned in Section 2.7. The peak areas of LF-CaP-Cs at different pH conditions were assessed. By comparing, the HPLC chromatogram of LF-CaP-Cs treated at different phosphate buffer pH conditions (pH 4.0, pH 5.0 and pH 7.4) it was observed that the peak area of LF-CaP-Cs treated with phosphate buffer pH 4.0 was higher (121,509 mAu) compared to pH 5.0 (25,525 mAu) and pH 7.4 (2350 mAu) respectively. The amount of LF released from LF-CaP-Cs with reference to different pH based buffers was found to be 2.860 µg/mL (pH 4.0), 1.124 µg/mL (pH 5.0) and 0.686 µg/mL (pH 7.4) respectively. The peak areas of LF-CaP-Cs found that in following order (pH 4.0 > 5.0 > 7.4) as shown in Fig. 5. These indicate the pH stimuli responsive behavior of LF-CaP-Cs at acidic environment mimicking within the cancerous cells. The enhanced release of LF at acidic environment may be due to the release of Ca^{2+} ions at acidic environment compared to alkaline environment (Pinto et al., 2011) Similarly, it has been reported that mesoporous silica-calcium phosphate hybrid

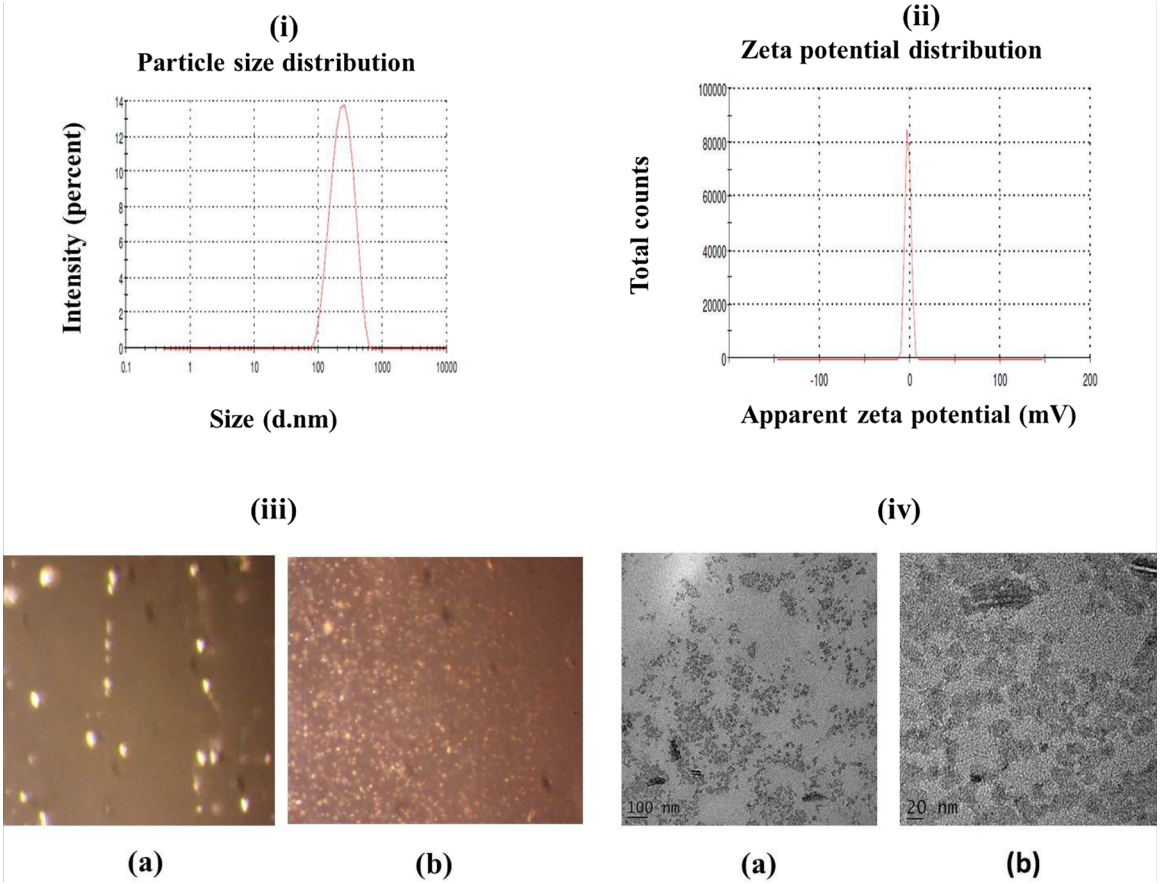

Fig. 3. *In-vitro* characterization of LF-CaP-Cs: (i) Particle size (ii) zeta potential (iii) light microscopic image of LF-CaP-Cs (a) and LF-Cs (b) at 10x magnification (iv) hr-TEM image of LF-CaP-Cs at magnifications of (a) 10x (b) 100x.

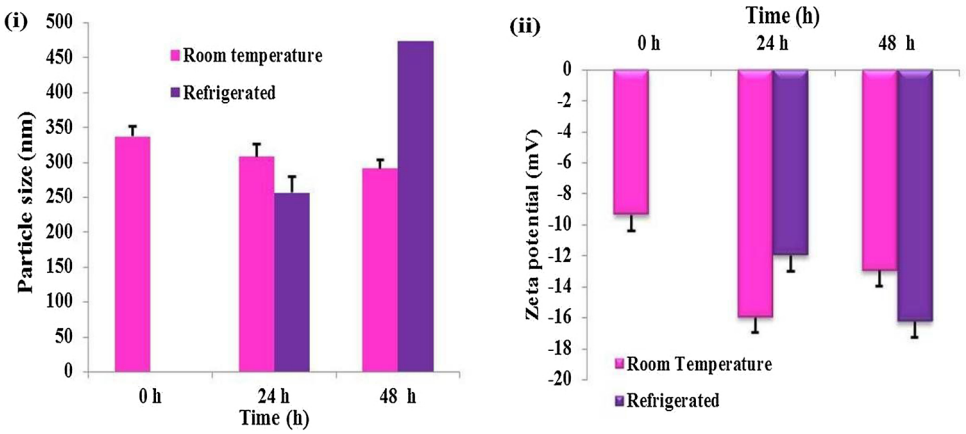

Fig. 4. *In-vitro* stability studies (i) particle size (ii) zeta potential for LF-CaP-Cs at room temperature and refrigerated conditions for.0–48 h.

nanoparticle effectively released up to 98.06% of doxorubicin at pH 4.5 compared to 61.28% at pH 5.5 due to easier dissolution of calcium phosphate and releases Ca^{2+} ions from the complex in acidic environment (Jiang et al., 2009). Further, calcium phosphate-polymer hybrid nanoparticle has been also reported for the co delivery of micro RNA inhibitor (miRi) and paclitaxel in triple negative breast cancer cells which showed that miRi gets released about 20.0% at pH 7.0 and 40.0% at pH 5.0 which showed with higher dissolution rate of calcium phosphate at acidic environment compared to physiological pH (Zhou et al., 2017).

3.10. In-vitro release behavior of LF-CaP-Cs at varying pHs

Results of LF release and LF release from LF-CaP-Cs were compared at pH 7.4 and pH 4.0. The release profile of LF from LF-CaP-Cs at pH 4.0 (84.04 ± 0.4%) was significantly higher than LF release at pH 7.4 (48.32 ± 1.6%) for 12 h (Fig. 6). Further it was observed, there was minimum amount of LF release was for free LF at both pH ranges of 7.4 and 4.0 at 12 h. The pH responsive characteristics of LF-CaP-Cs enable CaP for the site specific delivery of LF at lung cancer cells where slightly acidic environment was maintained (pH 4–6) whereas, the release gets limited at physiological pH. Recently, the pH responsive mesoporous silica calcium phosphate nanoparticle hybrid carrier had showed enhanced release of doxorubicin at pH 4.5 (98.84%) compared to pH 5.5

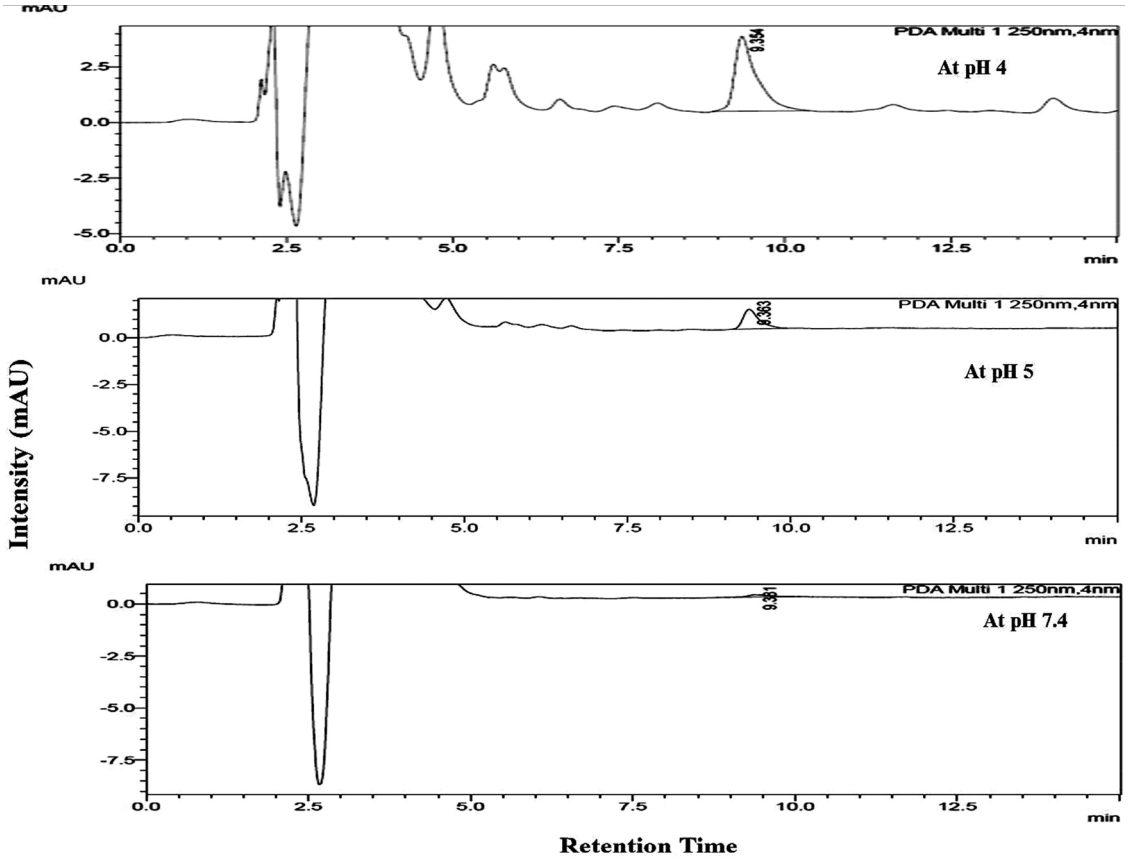

Fig. 5. HPLC chromatogram of pH stimuli responsive release profile for LF-CaP-Cs at different pH ranges (7.4, 5.0 and 4.0) showing higher peak intensity for LF (> 2.5) at pH 4.0, compared to pH 5.0 (< 2.5) and pH 7.4 (< 1.0).

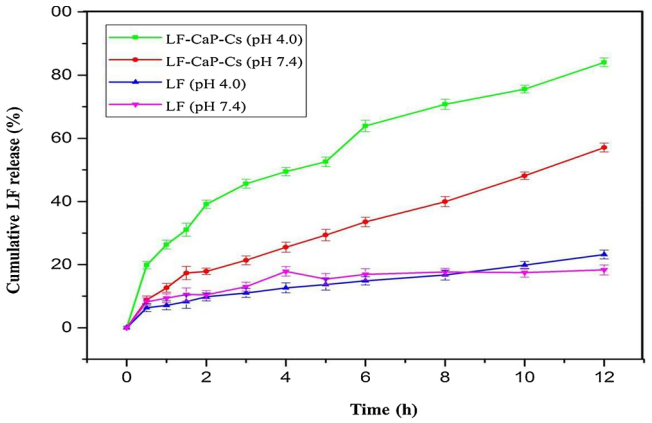

Fig. 6. *In-vitro* drug release profile for LF-CaP-Cs/LF at different pH conditions (pH 7.4 & pH 4.0). LF release was higher in pH 4.0 (84.04 ± 0.4%) compared to pH 7.4 (48.32 ± 1.6%) for LF-CaP-Cs at 12 h, whereas free LF doesn't showed significant release over the time period of 12 h.

(80.23%) (He et al., 2017a,b). Similarly, pH-sensitive zinc oxide quantum dots to deliver doxorubin in controlled manner by dissociation of the metal-drug complex to Zn^{2+} ions in acidic endosome/lysosome after cancer cells uptake (Cai et al., 2016). Similarly, pH-sensitive liposome loaded tyrosine kinase inhibitor afatinib were reported for its anticancer effect in human lung cancer cells (H1975). (Almurshedi et al., 2018).

3.11. Anti-angiogenesis assay (CAM assay)

The result of CAM assay showed better anti-angiogenic effect for LF-CaP-Cs (10 ng/disc) compared to LF-Cs (10 ng/disc) and LF (10 ng/disc). Initially CAM treated vessels was compared at 0^{th} and after 48^{th} h treatment and observed a decrease in CAM vessel density associated with damaged vessels which indicates the anti-angiogenic potential of developed LF-CaP-Cs (10 ng/disc) as shown in Fig. 7. Whereas, the individual CAM before treatment showed dense vessels with clear branching of blood vessels. In another setup the CAM treated LF-CaP-Cs (10 ng/disc) visualized after 3 h treatment period under optical microscope (MOTIC BA 310) showed disturbed/disintegrated individual CAM vessels compared to untreated individual CAM vessels as shown in Fig. 8. These results justify the potential anti-angiogenic activity of LF-CaP-Cs (10 ng/disc) revealed in terms of decrease in blood vessel diameter associated with decrease in CAM region. Previously, curcumin capped copper nanoparticles were reported for anti-angiogenic potential with significant reduction in length, size junction of tubule complexes in CAM (Kamble et al., 2016). It has been also reported that, diamond nanoparticles showed better anti-angiogenesis potential compared with graphite nanoparticles, graphene nanosheets, C60 fullerenes by inhibiting vascular endothelial growth factor thereby leads to decreasing the CAM thickness (Wierzbicki et al., 2013). Ginger extract is also reported to possess anti-angiogenic mediated anti-cancer activity with decreased in CAM vessel diameter (Bashir and Qadir, 2017).

3.12. Erythrocyte aggregation assay

Erythrocyte aggregation assay was performed to check toxicity of LF-CaP-Cs with erythrocytes. Results of erythrocyte aggregation assay showed that, untreated erythrocytes were spherical and appeared as individual cells whereas, after treatment with LF-CaP-Cs of phosphate buffer showed that, there was no aggregation found in erythrocytes (Fig. 9). Similarly, it was reported resveratrol loaded gelatin nanoparticles and vincristine loaded folic acid chitosan conjugated nanoparticles when treated with erythrocytes doesn't show any aggregation

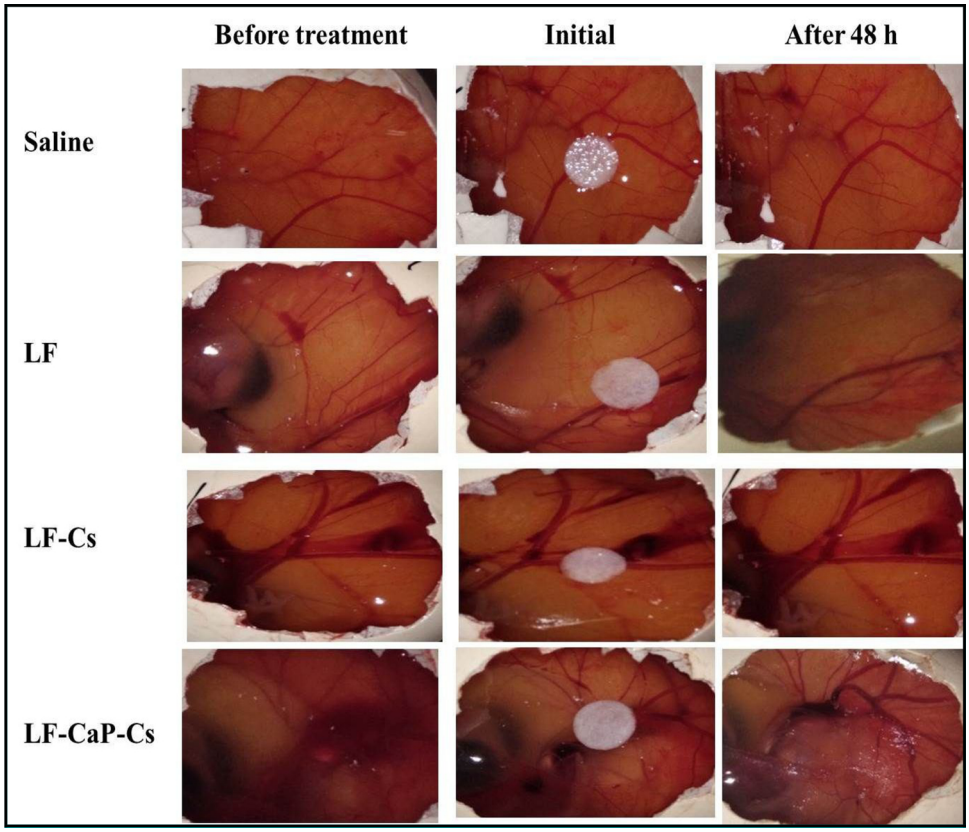

Fig. 7. Anti-angiogenesis assay: CAM treated with saline (control) doesn't show any morphological changes in CAM vessels. CAM treated with LF-CaP-Cs (10 ng/disc) showed better anti-angiogenic effect compared with LF (10 ng/disc) and LF-Cs (10 ng/disc).

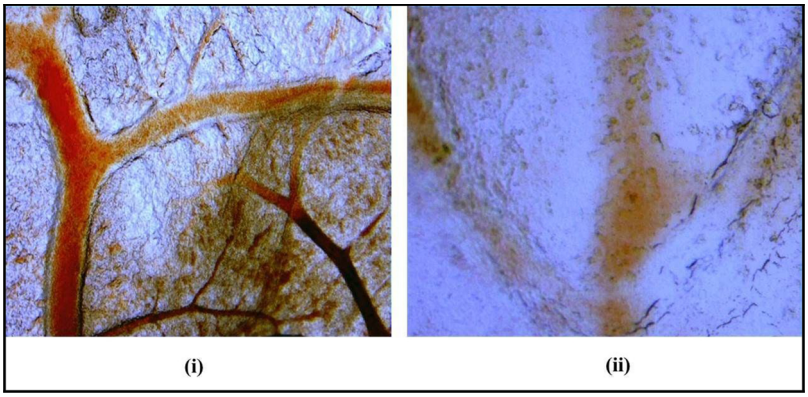

Fig. 8. (i) Individual CAM vessel before treatment showed clear and visible nascent blood vessels (ii) CAM vessel treated with LF-CaP-Cs (10 ng/disc) for 3 h showed destruction and disintegration of blood vessels.

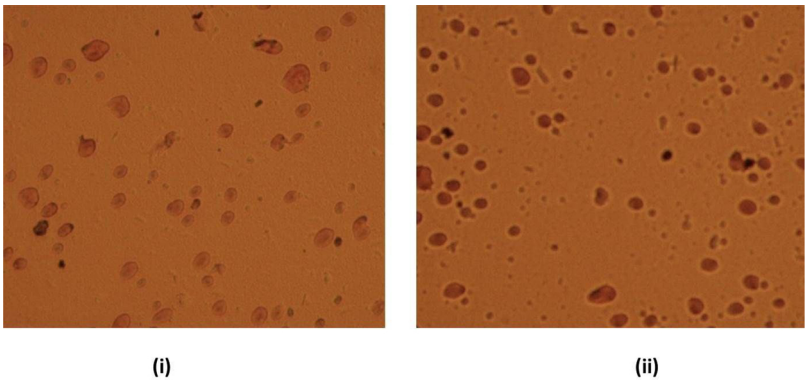

Fig. 9. Light microscopic image of Erythrocyte aggregation assay (i) Control erythrocytes (ii) Erythrocytes after treatment with LF-CaP-Cs at (10x magnification) showed that, no aggregation was observed.

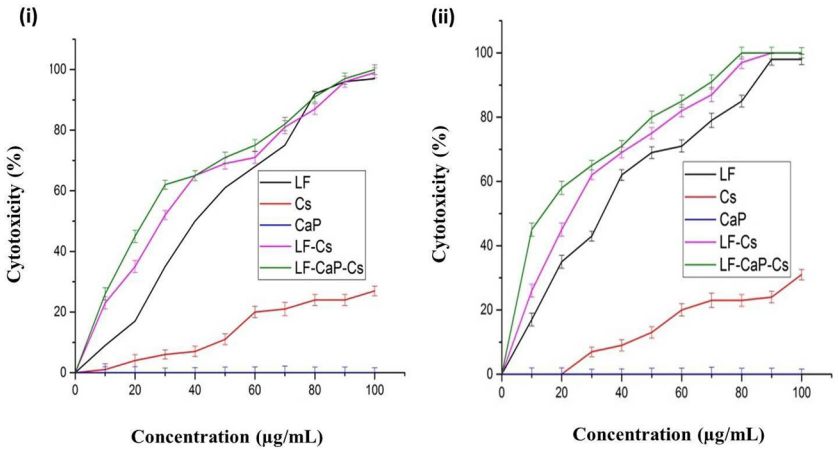

Fig. 10. *In-vitro* cytotoxic effect (MTT assay) of LF, CaP, Cs, LF-Cs and LF-CaP-Cs at different concentration (10–100 µg/mL) in human lung adenocarcinoma cell line (A549 cell line) for a treatment period of 24 h (i) and 48 h (ii) respectively. Data are presented as mean ± SD (n = 3). LF-CaP-Cs produces much significant higher cytotoxicity in A549 cells compared to LF-Cs and LF. Further, it was observed CaP and LF-Cs produce negligible cytotoxicity effect towards A549 cells. Results showed that LF-CaP-Cs showed statistically significant compared to Cs ($p < 0.05$).

of erythrocyte (Karthikeyan et al., 2013 & Kumar et al., 2018).

3.13. Hemolytic potential of LF-CaP-Cs

The hemolytic activity of LF-CaP-Cs was found to be (20.8 ± 0.87%, 16.9 ± 1.6% and 8.07 ± 1.24%) at the studied concentration of 100 ng/mL, 10 ng/mL, 1 ng/mL respectively. Further, free LF (100 ng/mL) showed 18.27% hemolysis activity and positive control triton X-100 showed 99.43% of hemolytic activity. Overall results showed that, hemolytic potential of LF-CaP-Cs (100 to 1 ng/mL) was < 25% which is the acceptable range for intravenous drug delivery application. Hence, the developed formulation may be safe for intravenous administration.

3.14. Cytotoxicity assay

The *in-vitro* anti-cancer effect of LF-CaP-Cs, LF, CaP, CaP-Cs and LF-Cs at the treatment period of 24 h and 48 h was measured by MTT assay and data's were shown in Fig. 10. Here, IC_{50} values were obtained by plotting the cell viability against the different concentrations. The results revealed that, cytotoxic effect of LF-CaP-Cs gets increased in a dose dependent manner (10–100 µg/mL) for both 24 and 48 h treatment periods (Fig. 10). Further, the mode of action and interaction of these LF-CaP-Cs, LF and LF-CaP-Cs with A549 cancer cells varied with their potency in the following order LF-CaP-Cs > LF > Cs > CaP. The cytotoxicity effect of LF-CaP-Cs was found to get increased at lower concentration compared to LF-Cs and free LF. However, the difference

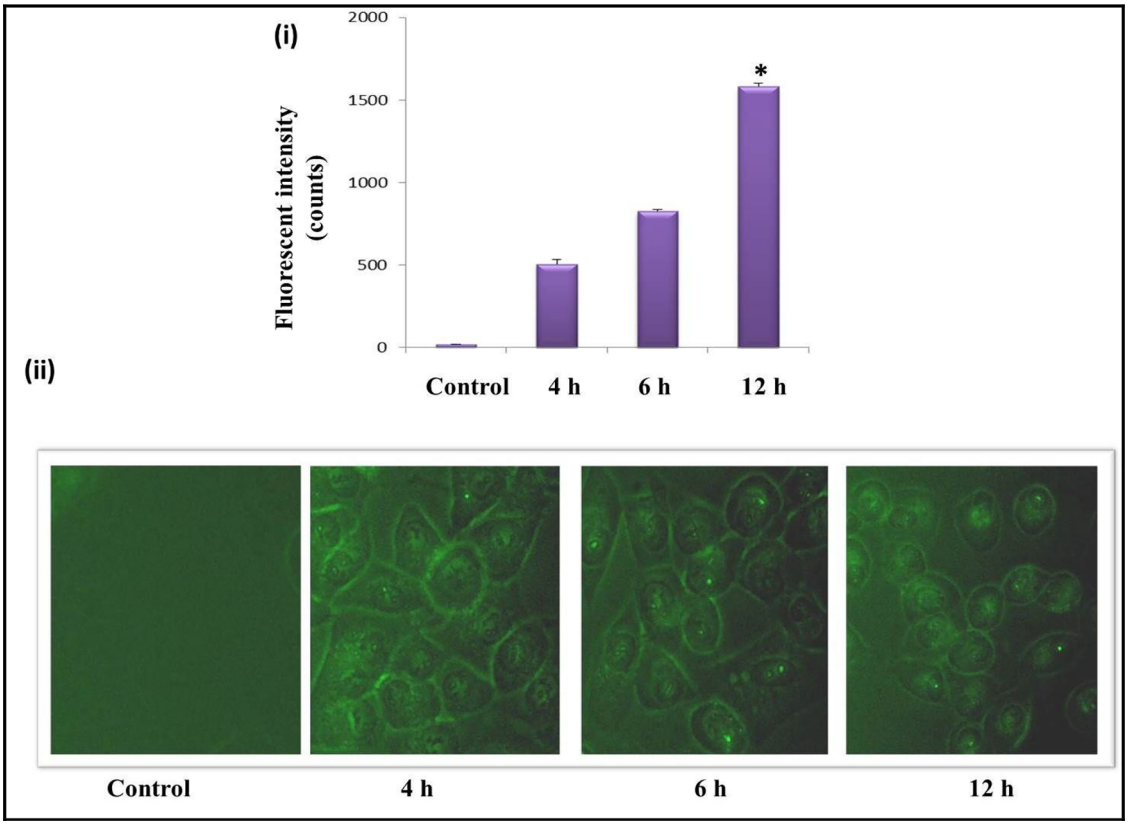

Fig. 11. (i) Mean fluorescent intensity of LF-CaP-Cs at different time intervals (4 h, 6 h and 12 h) using untreated cells used as control. LF-CaP-Cs showed statistically significant compared to control (*$p < 0.05$) at 12 h treatment period. (ii) Fluorescent images of A549 cells treated with FITC labelled LF-CaP-Cs at different time intervals 4 h, 6 h and 12 h. Results showed a time dependent cellular uptake in A549 cells.

was not significant at higher concentration. Blank Cs showed only 30 ± 2.1% μg/mL of cell death at the studied higher concentration for both 24 and 48 h. These result confirmed that, Cs used as a suitable carrier for LF has low toxicity. The IC_{50} of LF-CaP-Cs at 24 h was 28 ± 1.8 μg/mL, whereas, LF-Cs showed 35 ± 2.4 μg/mL at 24 h. The IC_{50} at 48 h was lower than that at 24 h which clearly indicates that, the cytotoxic effect is time as well as dose dependent. CaP doesn't produce any cytotoxicity in A549 cells whereas, CaP gets dissociated at acid environment (Xie et al., 2014) and releases the higher amount of LF to cancerous cells compared to normal cells thereby it may supports stimuli responsive (pH) release behavior contributing to the selective release of encapsulated LF in acidic tumor tissues. Thus, LF-CaP-Cs is biocompatible and it may be used as potential anti-cancer formulation for lung cancer treatment. This is the first report on LF for its anticancer activity in A549 human lung adenocarcinoma cell line. The above MTT assay results confirm that, the LF-CaP-Cs are biocompatible and may be utilized for applied in the biomedical field with good biocompatibility. Previously, it has been patented that LF can be used alone or combination with other endoplasmic reticulum stressor drugs which may act as autophagy inhibitor thereby it exerts its anticancer effect in Ba/F3 indicator cells expressing wild-type (p210) Bcr-Abl and mutant Bcr-Abl (McKenzie, 2011).

3.15. In-vitro cellular uptake of LF-CaP-Cs

The uptake of FITC labeled LF-CaP-Cs by A549 cells at different time intervals (4 h, 6 h, 12 h) were analyzed by inverted fluorescence microscopy and further the fluorescent intensities were measured using multimode micro plate reader. The extent of cellular uptake of LF-CaP-Cs gets monitored by comparing the mean fluorescence intensity of untreated cells. It has been observed LF-CaP-Cs gets localized around the cellular membrane of A549 cells after 4 h treatment period, whereas at 6 h, LF-CaP-Cs started to enter and accumulate inside cellular compartment (Fig. 11 ii). Further, LF-CaP-Cs may expected to completely enters inside the cytoplasm/nucleus which might show high fluorescence intensity at 12 h, suggesting time dependent cellular uptake and localization of LF-CaP-Cs in A549 cells. Overall the fluorescence intensity of LF-CaP-Cs get increased at 12 h (FI-1700) compared to the fluorescence intensities at 6 h (FI-800) and 4 h (FI-500) as shown in Fig. 11(i).

3.16. Acridine orange (AO) and ethidium bromide (EB) staining

Apoptotic effect during treatment with LF-CaP-Cs was characterized by different cellular and nuclear morphological changes such as cell shrinkage, nuclear condensation, DNA fragmentation, blebbing and formation of apoptotic bodies. The apoptotic mode of cell death is preferred compared to necrosis (Su et al., 2015). Necrosis is thought to be accidental, uncontrolled degeneration, while apoptosis is thought to represent a programmed cell death. The apoptotic morphology produced by LF-CaP-Cs and free LF was analyzed by using AO/EB in treated A549 human lung cancer cells. The results indicated that, the apoptotic morphologies induced at IC_{50} concentration of LF-CaP-Cs (28 ± 1.8 μg/mL) and free LF (40 ± 0.9 μg/mL) for 24 h were visualized under microscope. The results showed that, majority of cells undergone apoptotic pathway based cell death when treated with LF-CaP-Cs compared with LF. In free LF treated cells, most of the cells were in early apoptosis stage indicated by orange color whereas, LF- CaP-Cs showed late stage of apoptosis. LF-Cs also showed early stage of apoptosis and some at certain extend necrosis also. Under apoptosis conditions, the cells had undergone specific changes which include DNA fragmentation and nuclear condensation which may exhibits orange to red fluorescence. In case of necrosis, the cell death caused due to cytoplasmic swelling, destruction of organelles and destruction of

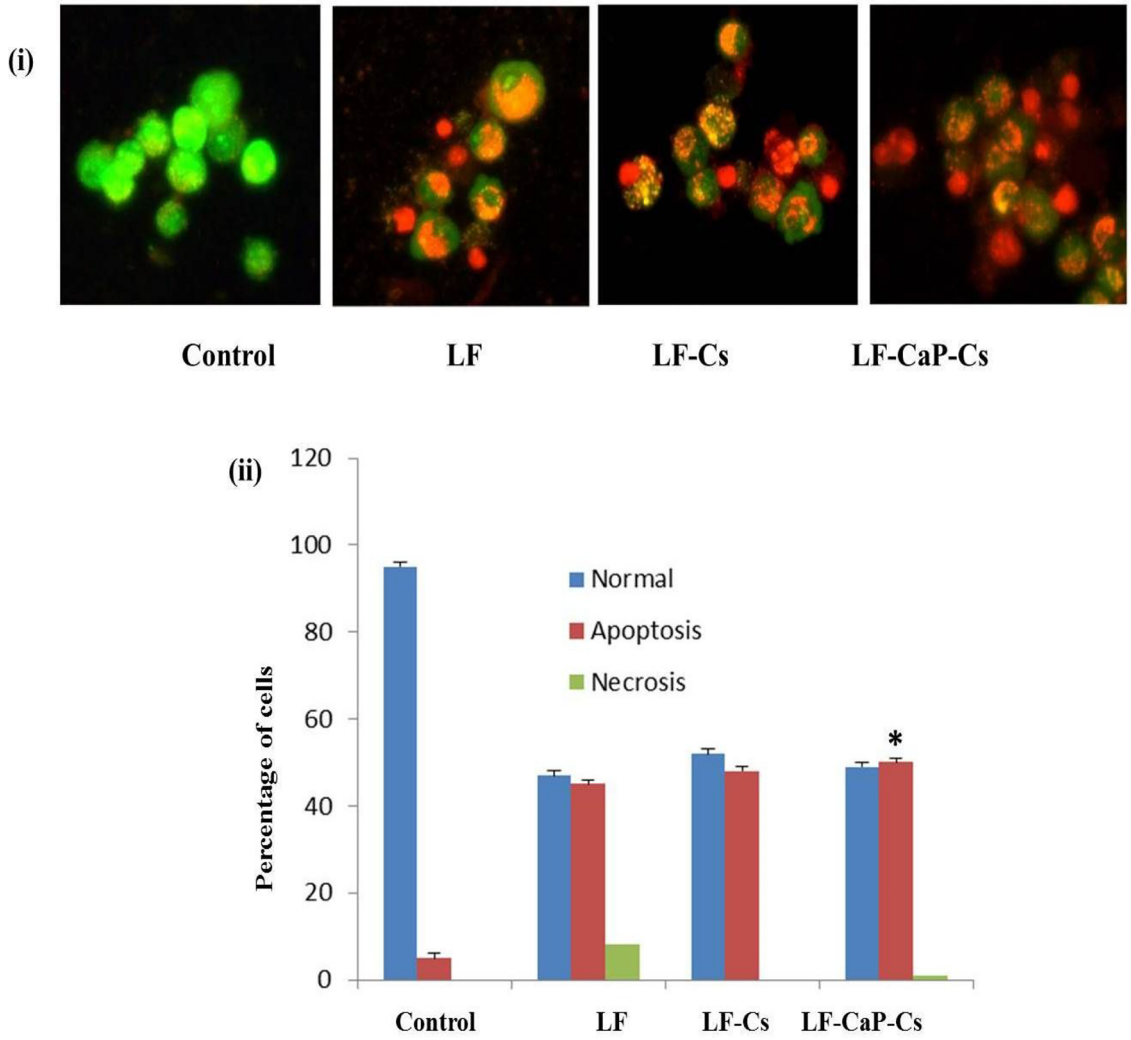

Fig. 12. (i) Fluorescent images of A549 cells under AO/EB staining of control cells (untreated) and Free LF(40 ± 0.9 μg/mL), LF-Cs (35 ± 2.4 μg/mL) and LF-CaP-Cs (28 ± 1.8 μg/mL) at IC_{50} concentrations 24 h treatment period (scale bar =10 μm) (ii) Percentage of normal, apoptotic and necrotic cells. LF-CaP-Cs showed statistically significant compared to control (*$p < 0.05$) in the aspects of apoptosis. Results showed that, LF-CaP-Cs showed apoptosis based cell death whereas LF showed apoptotic and necrosis based cell death.

plasma membrane. As per the present study, LF-CaP-Cs completely induce apoptosis, but free LF and LF-Cs induced apoptosis as well as necrosis to certain extent (Fig. 12i) Previously, it has been reported for that dioscin (natural steroid saponin) showing apoptotic based cell death in A549 cell towards lung cancer treatment (Wei et al., 2013).

Cancer therapeutics is important for effective management and treatment of various types of cancers. Cs have distinct properties such as high internal surface area with cubic, periodic three-dimensional structures, that can be easily accessible for hydrophilic, hydrophobic and amphiphilic molecules, enable their applications in diversified fields such as controlled delivery systems, food technology and healthcare products. In a cubic phase, lipid bilayers are arranged by contorting the bilayers into the shape of infinite periodic minimal surface. Cs have potential importance in terms of loading hydrophilic, hydrophobic and lipophilic drugs there by it serves as an alternative carrier to liposomes. Cs was also previously reported for wide range of cancer based studies, rheumatoid arthritis, siRNA delivery and for gene silencing strategies due to its unique features. Recently, it has been reported that Cs enhances the penetration effect in cells. Therefore, lipid phase of cubic phase structure mix with the subcutaneous lipids due to their similar structure (Lee et al., 2008, He et al., 2017a,b). LF is a highly lipophilic drug there by Cs may acts as suitable carrier, CaP supports the pH stimuli responsive behavior of LF. This type of approach may be useful for the effective treatment of cancer based drug delivery. The main precursors used in the present work was Cs synthesis were poloxamer 188 and cetyl palmitate which is biocompatible and non-toxic to human cells. Polyvinyl alcohol (0.25%) acts as stabilizing agent for the cubosomal preparation (LF-CaP-Cs). In general, pH responsive drug delivery system is reported as one of the promising strategy for the cancer treatment due to the slight acidic environment maintained in cancerous cells. Further, mechanistic calcium phosphate dissociation investigated at three different pH ranges (pH 4.0, 5.0 and 7.4) showed the CaP dissociation gets enhanced in acidic pH 4.0 which leads to the release of more amount LF compared to physiological pH 7.4. The pH sensitive LF release was further confirmed by *in-vitro* release profile for LF-CaP-Cs at pH 7.4 and pH 4.0. Moreover, it was proven that, LF-CaP-Cs showed better cytotoxic potential with high cellular uptake towards human lung adenocarcinoma A549 cell line compared to LF-Cs and free LF in dose dependent manner. It has been reported, the blank Cs was produce negligible cytotoxicity towards cancerous cells and our studies revealed the same results (Abdel-Bar and EL Basset, 2017). In addition, our results have shown that, CaP doesn't produce any cytotoxicity towards A549 cell lines. The main advantages towards Cs based formulation approach was minimization of side effects of the toxic drug with improved efficacy at low dose.

4. Conclusion

To conclude, the developed LF-CaP-Cs may acts as better therapeutic potential for the effective treatment of lung cancer. The developed LF-CaP-Cs showed lower particle size with higher encapsulation efficiency. Based on the supportive *in-vitro* results, LF-Cap-Cs showed better anticancer activity based on the pH responsive mechanism against human adenocarcinoma cell line A549 which may improves the efficacy of LF at lower doses in the form of LF-CaP-Cs. Overall the results showed that, Cs may acts as suitable carrier for lipophilic drugs such as LF and further *in-vivo* studies supported with molecular biology studies required to evaluate *in-vivo* antitumor activity.

Conflict of interest

The authors don't declare any conflict of interest.

Acknowledgements

The authors gratefully acknowledge Department of Science and Technology (GoI), New Delhi supported National Facility for Drug Development for Academia, Pharmaceutical and Allied Industries (NFDD) (Ref No. VI- D&P/349/10-11/TDT/1 Dt: 21.10.2010). One of the authors Ms. S. Vaidevi gratefully acknowledges the financial support (Senior Research Fellowship) received from Indian council of medical research, New Delhi (Ref No. 45/20/2018/NAN/BMS. Dt.30.05.2018). Authors acknowledge Madras Pharma, Chennai for providing gift drug sample of Lumefantrine.

References

Abdel-Bar, H.M., EL Basset, R.A., 2017. Endocytic pathways of optimized resveratrol cubosomes capturing into human hepatoma cells. Biomed. Pharmacother. 93, 561–569.
Almurshedi, A.S., Radwan, M., Omar, S., Alaiya, A.A., Badran, M.M., Elsaghire, H., Saleem, I.Y., Hutcheon, G.A., 2018. A novel pH-sensitive liposome to trigger delivery of afatinib to cancer cells: impact on lung cancer therapy. J. Mol. Liq. 259, 154–166.
Amreddy, N., Babu, A., Muralidharan, R., Munshi, A., Ramesh, R., 2017. Polymeric nanoparticle-mediated gene delivery for lung cancer treatment. Top. Curr. Chem. (Cham) 375 (2), 35.
Aweeka, F.T., German, P.I., 2008. Clinical pharmacology of Artemisinin-based combination therapies. Clin. Pharmacokinet. 47 (2), 91–102.
Bashir, M.F., Qadir, M.I., 2017. Effect of ginger extract on angiogenesis using CAM assay. Bangladesh J. Pharmacol. 12, 348–353.
Bilewicz, R., Nazaruk, E., Majkowska-Pilip, A., Bilewicz, R., 2017. Lipidic cubic phase nanoparticles-cubosomes for improved efficiency of drug delivery to cancer cells. ChemPlusChem 82 (4), 570–575.
Bodratti, A.M., Alexandridis, P., 2018. Formulation of poloxamers for drug delivery. J. Funct. Biomater. 9 (1), E11.
Cai, X., Luo, Y., Zhang, W., Du, D., Lin, Y., 2016. pH-sensitive ZnO quantum dots-doxorubicin nanoparticles for lung cancer targeted drug delivery. ACS Appl. Mater. Interfaces 8 (34), 22442–22450.
Denholm, R., Schuz, J., Straif, K., Jockel, K.H., Brenner, D.R., De Matteis, S., Boffetta, P., Guida, F., Bruske, I., Wichmann, H.E., Landi, M.T., Caporaso, N., Siemiatycki, J., Ahrens, W., Pohlabeln, H., Zaridze, D., Field, J.K., McLaughlin, J., Demers, P., Szeszenia-Dabrowska, N., Lissowska, J., Rudnai, E.P., Fabianova, Dumitru, R.S., Bencko, V., Foretova, L., Janout, V., Kendzia, B., Peters, S., Behrens, T., Vermeulen, R., Bruning, T., Kromhout, H.A., Olsson, C., 2014. Is previous respiratory disease a risk factor for lung cancer? Am. J. Respir. Crit. Care Med. 190 (5), 549–559.
Ezzet, F., 2000. Pharmacokinetics and pharmacodynamics of lumefantrine (benflumetol) in acute falciparum malaria. Antimicrob. Agents Chemother. 44 (3), 697–704.
Frede, A., Neuhaus, B., Knuschke, T., Wadwa, M., Kollenda, S., Klopfleisch, R., Hansen, W., Buer, J., Bruder, D., Epple, M., Westendorf, A.M., 2017. Local delivery of siRNA-loaded calcium phosphate nanoparticles abates pulmonary inflammation. Nanomedicine 13 (8), 2395–2403.
Gaymalov, Z.Z., Yang, Z., Pisarev, V.M., Alakhov, V.U., Kabanov, A.V., 2009. The Effect of the nonionic block copolymer pluronic P85 on gene expression in mouse muscle and antigen presenting cells. Biomaterials 30 (6), 1232–1245.
Hadjicharalambous, C., Kozlova, D., Sokolova, V., Epple, M., Chatzinikolaidou, M., 2015. Calcium phosphate nanoparticles carrying BMP-7 plasmid DNA induce an osteogenic response in MC3T3-E1 pre-osteoblasts. J. Biomed. Mater. Res. A 103 (12), 3834–3842.
He, H., Rahimi, K., Zhong, M., Mourran, A., Luebke, D.R., Nulwala, H.B., Moller, M., Matyjaszewski, K., 2017a. Cubosomes from hierarchical self-assembly of poly (ionic liquid) block copolymers. Nat. Commun. 8, 14057.
He, Y., Zeng, B., Liang, S., Long, M., Xu, H., 2017b. Synthesis of pH-responsive biodegradable mesoporous silica calcium phosphate hybrid nanoparticle as a high potential drug carrier. ACS Appl. Mater. Interfaces 9 (51), 44402–44409.
Honary, S., Zahir, F., 2013. Effect of zeta potential on the properties of nano-drug delivery systems - a review. Trop. J. Pharm. Res. 12 (2), 265–273.
Jiang, J., Oberdorster, G., Biswas, P., 2009. Characterization of size, surface charge and agglomeration state of nanoparticle dispersions for toxicological studies. J. Nanopart. Res. 11, 77–89.
Jitendra, Sharma, P.K., Bansal, S., Banik, A., 2011. Non-invasive routes of proteins and peptides drug delivery. Indian J. Pharm. Sci. 73 (4), 367–375.
Kamble, S., Utage, B., Mogle, P., Kamble, R., Hese, S., Dawane, B., Gacche, R., 2016. Evaluation of curcumin capped copper nanoparticles as possible inhibitors of human breast cancer cells and angiogenesis: a comparative study with native curcumin. AAPS Pharm. Sci. Tech. 17 (5), 1030–1041.
Karthikeyan, S., Rajendra Prasad, N., Ganamani, A., Balamurugan, E., 2013. Anticancer activity of resveratrol-loaded gelatin nanoparticles on NCI-H460 non-small cell lung cancer cells. Biomed. Prev. Nutr. 3, 64–73.
Khan, M.A., Wu, V.M., Ghosh, S., Uskokovi, V., 2016. Gene delivery using calcium phosphate nanoparticles: optimization of the transfection process and the effects of citrate and poly (L-lysine) as additives. J. Colloid Interface Sci. 471, 48–58.
Kim, H., Leal, C., 2015. Cuboplexes: topologically active siRNA delivery. ACS Nano 9 (10), 10214–10226.
Kokwaro, G., Mwai, L., Nzila, A., 2007. Artemether/lumefantrine in the treatment of uncomplicated falciparum malaria. Expert Opin. Pharmacother. 8 (1), 75–94.
Kumar, N., Salar, R.K., Prasad, M., Ranjan, K., 2018. Synthesis, characterization and anticancer activity of vincristine loaded folic acid-chitosan conjugated nanoparticles on NCI-H460 non-small cell lung cancer cell line. EJBAS 5 (1), 87–99.
Lee, K.W., Nguyen, T.H., Hanley, T., Boyd, B.J., 2009. Nanostructure of liquid crystalline matrix determines *in-vitro* sustained release and *in-vivo* oral absorption kinetics for hydrophilic model drugs. Int. J. Pharm. 365 (1-2), 190–199.
Lee, M.S., Lee, J.E., Byun, E., Kim, N.W., Lee, K., Lee, H., 2014. Target-specific delivery of siRNA by stabilized calcium phosphate nanoparticles using dopa-hyaluronic acid conjugate. J. Control. Release 192, 122–130.
Mani, D., Haigentz, M.J., Aboulafia, D.M., 2012. Lung cancer in HIV infection. Clin. Lung Cancer 13 (1), 6–13.
McKenzie, D.T., Use of lumefantrine and related compounds in the treatment of cancer, US 2011/0300137 A1.
Nasr, M., Ghorab, M.K., Abdelazem, 2015. A. *In-vitro* and *in-vivo* evaluation of cubosomes containing 5-fluorouracil for liver targeting. Acta Pharm. Sin. B 5 (1), 79–88.
Neumann, S., Kovtun, A., Dietzel, I.D., Epple, M., Heumann, R., 2009. The use of size-defined DNA-functionalized calcium phosphate nanoparticles to minimize intracellular calcium disturbance during transfection. Biomaterials 30 (35), 6794–6802.
Nielsen, L.S., Bælum, J., Rasmussen, J., Dahl, S., Olsen, K.E., Albin, M., Hansen, N.C., Sherson, D., 2014. Occupational asbestos exposure and lung cancer - A systematic review of the literature. Arch. Environ. Occup. Health 69 (4), 191–206.
Noronha, V., Pinninti, R., Patil, V.M., Joshi, A., Prabhash, K., 2016. Lung cancer in the Indian subcontinent. South Asian J. Cancer 5 (3), 95–103.
Pan, X., Han, K., Peng, X., Yang, Z., Qin, L., Zhu, C., Huang, X., Shi, X., Dian, L., Lu, M., Wu, C., 2013. Nanostructured cubosomes as advanced drug delivery system. Curr. Pharm. Des. 19 (35), 6290–6297.
Peng, X., Wen, X., Pan, X., Wang, R., Chen, B., Wu, C., 2010. Design and *in-vitro* evaluation of capsaicin transdermal controlled release cubic phase gels. AAPS Pharm. Sci. Tech. 11 (3), 1405–1410.
Pinto, O.A., Tabakovic, A., Goff, T.M., Liu, Y., Adair, J.H., 2011. Calcium phosphate and calcium phosphosilicate mediated drug delivery and imaging. Intracell. Deliv. 5, 713–744.
Powell, H.A., Iyen-Omofoman, B., Baldwin, D.R., Hubbard, R.B., Tata, L.J., 2013. Chronic obstructive pulmonary disease and risk of lung cancer: the importance of smoking and timing of diagnosis. J. Thorac. Oncol. 8 (1), 6–11.
Ribatti, D., 2016. The chick embryo chorioallantoic membrane (CAM) assay. Reprod. Toxicol. 0890–6238.
Ridge, C.A., McErlean, A.M., Ginsberg, M.S., 2013. Epidemiology of lung cancer. Semin. Intervent. Radiol. 30 (2), 93–98.
Rim, H.P., Min, K.H., Lee, H.J., Jeong, S.Y., Lee, S.C., 2011. pH-tunable calcium phosphate covered mesoporous silica nano containers for intracellular controlled release of guest drugs. Angew. Chem. Int. Ed. Engl. 50 (38), 8853–8857.
Rosenblatt, K.M., Bunjes, H., 2017. Evaluation of the drug loading capacity of different lipid nanoparticle dispersions by passive drug loading. Eur. J. Pharm. Biopharm. 117, 49–59.
Rotan, O., Severin, K.N., Popsel, S., Peetsch, A., Merdanovic, M., Ehrmann, M., 2017. Uptake of the proteins HTRA1 and HTRA2 by cells mediated by calcium phosphate nanoparticles. Beilstein J. Nanotechnol. 8, 381–393.
Roy, I., Mitra, S., Maitra, A., Mozumdar, S., 2003. Calcium phosphate nanoparticles as novel non-viral vectors for targeted gene delivery. Int. J. Pharm. 250 (1), 25–33.
Sahdev, P., Podaralla, S., Kaushik, R.S., Perumal, O., 2013. Calcium phosphate nanoparticles for transcutaneous vaccine delivery. J. Biomed. Nanotechnol. 9 (1), 132–141.
Santander-Ortega, M.J., Csaba, M.J., Alonso, N., Ortega-Vinuesa, J.L., Bastos-Gonzalez, D., 2007. Stability and physicochemical characteristics of PLGA, PLGA: poloxamer and PLGA: poloxamine blend nanoparticles: a comparative study. Colloids Surf. A Physicochem. Eng. Asp. 296 (1-3), 132–140.
Schwiertz, J., Wiehe, A., Grafe, S., Gitter, B., Epple, M., 2009. Calcium phosphate nanoparticles as efficient carriers for photodynamic therapy against cells and bacteria. Biomaterials 30, 3324–3331.
Semete, B., Booysen, L., Lemmer, Y., Kalombo, L., Katata, L., Verschoor, J., Swai, H.S.,

2010. *In-vivo* evaluation of the biodistribution and safety of PLGA nanoparticles as drug delivery systems. Nanomedicine 6 (5), 662–671.
Semete, B., Booysen, L., Kalombo, L., Ramalapa, B., Hayeshi, R., Swai, H.S., 2012. Effects of protein binding on the biodistribution of PEGylated PLGA nanoparticles post oral administration. Int. J. Pharm. 424 (1-2), 115–120.
Sethi, T.K., El-Ghamry, M.N., Kloecker, G.H., 2012. Radon and lung cancer. Clin. Adv. Hematol. Oncol. 10 (3), 157–164.
Sezaki, H., Hashida, M., 2011. Macromolecules as drug delivery systems. Directed Drug Deliv. 189–208.
Sharma, N., Madan, P., Lin, S., 2016. Effect of process and formulation variables on the preparation of parenteral paclitaxel-loaded biodegradable polymeric nanoparticles: a co-surfactant study. Asian J. Pharm. Sci. 11, 404–416.
Shubhra, Q.T.H., Toth, J., Gyenis, J., Feczko, T., 2014. Poloxamers for surface modification of hydrophobic drug carriers and their effects on drug delivery. Polym. Rev. 54 112-138L.
Sokolova, V., Kozlova, D., Knuschke, T., Buer, J., Westendorf, A.M., Epple, M., 2013. Mechanism of the uptake of cationic and anionic calcium phosphate nanoparticles by cells. Acta Biomater. 9 (7), 7527–7535.
Spector, D.L., Goldman, R.D., Leinwand, L.A., 1998. Cell: a laboratory manual, culture and biochemical analysis of cells. Cold Spring Harbor 134 (1-34), 9.
Su, Z., Yang, Z., Xu, Y., Chen, Y., Yu, Q., 2015. Apoptosis, autophagy, necroptosis and cancer metastasis. Mol. Cancer 14, 48.
Tian, J.L., Zhao, Y.Z., Jin, Z., Lu, C.T., Tang, Q.Q., Xiang, Q., Sun, C.Z., Zhang, L., Xu, Y.Y., Gao, H.S., Zhou, Z.C., Li, X.K., Zhang, Y., 2010. Synthesis and characterization of poloxamer 188-grafted heparin copolymer. Drug Dev. Ind. Pharm. 36 (7), 832–838.
Tian, Y., Li, J.C., Zhu, J.X., Zhu, N., Zhang, H.M., Liang, L., Sun, L., 2017. Folic acid-targeted etoposide cubosomes for theranostic application of cancer cell imaging and therapy. Med. Sci. Monit. 23, 2426–2435.
Travassos, M.A., Laufer, M.K., 2009. Resistance to antimalarial drugs: molecular, pharmacologic, and clinical considerations. Pediatr. Res. 65 (5 Pt 2), 64R–70R.
Turner, M.C., Krewski, D., Chen, Y., Pope, C.A., Gapstur, S., Thun, M.J., 2011. Radon and lung cancer in the American cancer society cohort. Cancer Epidemiol. Biomarkers Prev. 20 (3), 438–448.
Wei, Y., Xu, Y., Han, X., Qi, Y., Xu, L., Xu, Y., Yin, L., Sun, H., Liu, K., Peng, J., 2013. Anticancer effects of dioscin on three kinds of human lung cancer cell lines through inducing DNA damage and activating mitochondrial signal pathway. Food Chem. Toxicol. 59, 118–128.
White, N.J., 1999. Clinical pharmacokinetics and pharmacodynamics and pharmacodynamics of Artemether-lumefantrine. Clin. Pharmacokinet. 37, 105–125.
Wierzbicki, M., Sawosz, E., Grodzik, M., Prasek, M., Jaworski, S., Chwalibog, A., 2013. Comparison of anti-angiogenic properties of pristine carbon nanoparticles. Nanoscale Res. Lett. 8 (1), 195.
Xie, Y., Qiao, H., Su, Z., Chen, M., Ping, Q., Sun, M., 2014. PEGylated carboxymethyl chitosan/calcium phosphate hybrid anionic nanoparticles mediated hTERT siRNA delivery for anticancer therapy. Biomaterials. 35 (27), 7978–7991.
Yaghmur, A., Glatter, O., 2009. Characterization and potential applications of nanostructured aqueous dispersions. Adv. Colloid Interface Sci. 147-148, 333–342.
Yu, Y.H., Liao, C.C., Hsu, W.H., Chen, H.J., Liao, W.C., Muo, C.H., Sung, F.C., Chen, C.Y., 2011. Increased lung cancer risk among patients with pulmonary tuberculosis: a population cohort study. J. Thorac. Oncol. 6 (1), 32–37.
Zarrintaj, P., Ahmadi, Z., Saeb, M.R., Mozafari, M., 2018. Poloxamer-based stimuli-responsive biomaterials. Mater. Today Proc. 5 (7), 15516–15523.
Zhang, M., Ishii, A., Nishiyama, N., Matsumoto, S., Ishii, T., Yamasaki, Y., Kataoka, K., 2009. PEGylated calcium phosphate nano composites as smart environment-sensitive carriers for siRNA delivery. Adv. Mater. 21, 3520–3525.
Zhen, G., Hinton, T.M., Muir, B.W., Shi, S., Tizard, M., Glycerol, K., Tizard, M., McLean, K.M., Hartley, P.G., Gunatillake, P., 2012. Monooleate-based nanocarriers for siRNA delivery in-vitro. Mol. Pharmaceutics 9 (9), 2450–2457.
Zhou, Z., Kennell, C., Lee, J.Y., Leung, Y.K., Tarapore, P., 2017. Calcium phosphate-polymer hybrid nanoparticles for enhanced triple negative breast cancer treatment via co-delivery of paclitaxel and miR-221/222 inhibitors. Nanomedicine 13 (2), 403–410.